# Observation of In concentration variations in InGaN/GaN quantum-well heterostructures by scanning capacitance microscopy

X. Zhou and E. T. Yu[a)]
*Department of Electrical and Computer Engineering, University of California, San Diego, La Jolla, California 92093-0407*

D. I. Florescu, J. C. Ramer, D. S. Lee, S. M. Ting, and E. A. Armour
*Veeco TurboDisc Operations, 394 Elizabeth Avenue, Somerset, New Jersey 08873*

(Received 15 February 2005; accepted 5 April 2005; published online 12 May 2005)

Scanning capacitance microscopy and spectroscopy have been used to analyze nanoscale variations in electronic properties in $In_{0.15}Ga_{0.85}N/GaN$ quantum-well structures grown by metalorganic chemical vapor deposition. Scanning capacitance imaging reveals that localized regions within the $In_{0.15}Ga_{0.85}N$ quantum well, up to ~25 nm in radius and present at densities in the range of $10^9-10^{10}$ $cm^{-2}$, exhibit markedly increased electron accumulation relative to surrounding areas. Spatially resolved scanning capacitance spectroscopy combined with numerical simulations indicates that these regions of enhanced electron accumulation are characterized by locally increased In concentration in the quantum well. The presence of these localized In-rich regions is correlated with reported observations of increased luminescence efficiency, presumably due to carrier localization and consequently enhanced radiative recombination, in very similarly grown samples. In addition, these results demonstrate the ability, using a surface characterization technique, to image variations in composition in a subsurface quantum well with nanoscale spatial resolution. © *2005 American Institute of Physics*. [DOI: 10.1063/1.1929871]

$In_xGa_{1-x}N/GaN$ quantum-well structures are of current interest for nitride semiconductor-based visible light emitters, including both light-emitting diodes and laser diodes.[1,2] Optimization of emission efficiencies in such devices requires a detailed understanding of the local, nanoscale structure and associated electronic properties in the $In_xGa_{1-x}N/GaN$ quantum-well region. For example, the polarization-induced electric field in the quantum well has a large impact on the degree of wave function overlap between electrons and holes and, therefore, directly influences recombination efficiency.[3] In addition, evidence of compositional inhomogeneities such as clustering or phase separation has been reported in $In_xGa_{1-x}N/GaN$ quantum-well structures,[4–6] and these inhomogeneities are believed to play a major role in the attainment of high emission efficiencies.[1,7] However, direct characterization of the local, nanoscale electronic and optical properties associated with phenomena such as In clustering remains a challenge.

We have used scanning capacitance microscopy (SCM)[8,9] and spectroscopy to characterize local, nanometer-scale variations in carrier concentration in an $In_{0.15}Ga_{0.85}N/GaN$ quantum-well structure, which we interpret as arising from the presence of nanoscale In-rich regions in the $In_xGa_{1-x}N$ quantum well. Increased electron accumulation in nanometer-scale areas of the quantum well is observed, with the density of these regions being in good agreement with that determined in separate electron microscopy studies.[10] The observed evolution in SCM contrast with bias voltage is consistent with that expected on the basis of numerical simulations for structures with varying In concentration in the quantum well, and cannot be explained as a consequence of the presence of alternate structural variations such as fluctuations in quantum-well thickness. The ability to observe effects of nanoscale In compositional variations in a subsurface quantum well is noteworthy given the general difficulty of directly imaging subsurface electronic and structural properties in semiconductors and the significance of In clustering in particular in affecting efficiencies of nitride-based light emitters.

The sample employed in these studies, whose structure is shown schematically in Fig. 1, was grown by metalorganic chemical vapor deposition (MOCVD) on a *c*-plane sapphire substrate using a Veeco TurboDisc E300 GaNzilla platform.

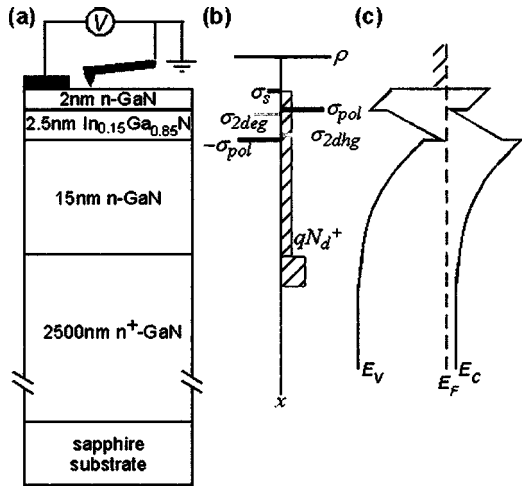


FIG. 1. (a) Schematic diagram of $In_{0.15}Ga_{0.85}N/GaN$ quantum-well structure showing contact and measurement geometry; (b) schematic diagram of electrostatic charge distribution. Sheet charges corresponding to the two-dimensional electron gas ($\sigma_{2deg}$) and two-dimensional hole gas ($\sigma_{2dhg}$) are dependent on bias voltage and therefore indicated in grey; (c) schematic energy-band-edge diagram for the $In_{0.15}Ga_{0.85}N/GaN$ quantum-well structure.

[a)]Electronic mail: ety@ece.ucsd.edu

 

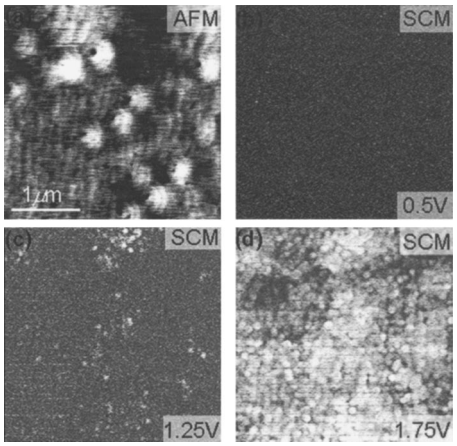


FIG. 2. (a) Topographic image and (b)–(d) scanning capacitance images of the $In_{0.15}Ga_{0.85}N/GaN$ quantum-well sample. Data scale is 2 V for (b), (c), and 4 V for (d).

A 15 nm GaN layer was grown on 2.5 $\mu$m undoped ($n \sim 5 \times 10^{16}$ cm$^{-3}$) GaN grown at 1080 °C. The quantum well region consisted of a 2.5 nm $In_xGa_{1-x}N$ well with $x \sim 15\%$ grown at 750 °C, followed by a 2.0 nm GaN cap grown at the same temperature. The $In_xGa_{1-x}N$ well was grown using 37 $\mu$mol/min of trimethylindium and 26 $\mu$mol/min of triethylgallium and the growth time was 90 s. The proximity of the quantum-well region to the sample surface enabled very high spatial resolution to be achieved in SCM characterization.[11] All samples were cleaned with trichloroethylene, acetone, and methanol in an ultrasonic bath, followed by a rinse in isopropanol and then acid cleaning using $HCl:H_2O$ (1:1) prior to processing or imaging. Ohmic contacts were fabricated on all samples by deposition of 33 nm Ti/77 nm Al/33 nm Ti/88 nm Au followed by annealing at 650 °C for 3 min. Scanning capacitance microscopy and spectroscopy were performed in a Digital Instruments/Veeco Nanoscope IIIa Dimension 3100 s scanning probe microscopy system using Co/Cr-coated tips with a nominal tip radius of 25–50 nm.

To assist in the interpretation of scanning capacitance data, numerical simulations of capacitance–voltage spectra were performed using a one-dimensional Poisson–Schrodinger solver[12] with band offsets and polarization charge densities at the $In_{0.15}Ga_{0.85}N/GaN$ interfaces derived from experimentally measured values.[13] The capacitance behavior observed in these simulations was confirmed by capacitance–voltage spectroscopy performed on large-area Schottky diodes. The macroscopic capacitance–voltage behavior observed, and its interpretation, were very similar to those reported previously in studies of similar $In_xGa_{1-x}N/GaN$ quantum-well structures.[11] The relevant regime of behavior in the current studies is that corresponding to moderate positive tip bias voltages, for which capacitance associated with electron accumulation in the quantum well is observed.

Figure 2 shows representative 3 $\mu$m × 3 $\mu$m topographic and scanning capacitance images for a series of tip bias voltages ranging from 0.5 to 1.75 V. Monolayer steps ~2.5–3 Å in height, indicative of step-flow growth, are clearly visible in the topographic image, as are spiral growth hillocks associated with screw-component dislocations.[14] Surface depressions associated with threading dislocations are visible with an approximate density of $3 \times 10^9$ cm$^{-2}$. Local electronic structure is revealed in SCM imaging. With the probe tip biased at 0.5 V relative to the sample, little contrast is evident in the SCM image. At 1.25 V, isolated, approximately circular areas 30–50 nm in radius with increased SCM signal levels are observed, and at 1.75 V these and additional regions of increased SCM signal level are much more evident; the radius of the features visible at 1.25 V increases to 35–55 nm at 1.75 V, suggesting a corresponding expansion of the area within which electron accumulation occurs. The actual size of these features is, of course, considerably smaller than the size observed in the image due to tip convolution and sample depletion effects. Very approximately, the observed radius of a given feature will be the sum of the probe tip radius (typically 25–50 nm), the depletion depth within the sample (a few nm in our studies due to the proximity of the quantum well to the surface), and the actual feature size, which based on this approach we estimate to be 25 nm or smaller. The density of these features is $\sim 2 \times 10^9$ cm$^{-2}$ at 1.25 V bias and $\sim 8 \times 10^9$ cm$^{-2}$ at 1.75 V. At 2 and 2.25 V (not shown), the image contrast associated with these features largely subsides.

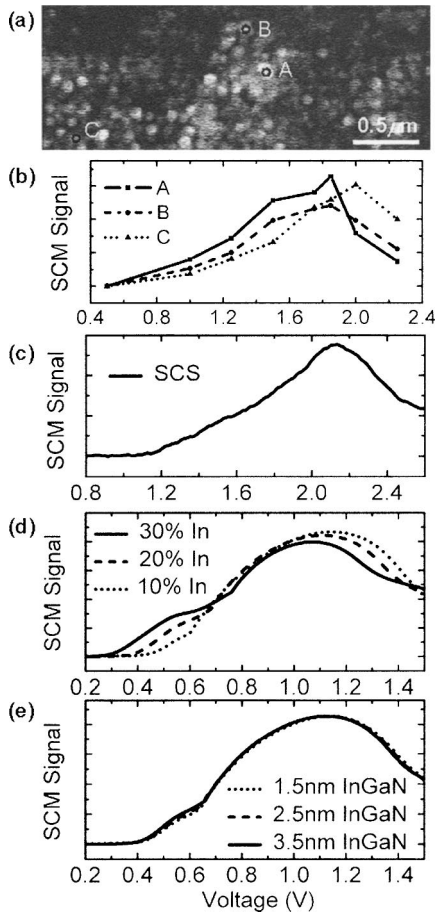


FIG. 3. (a) Scanning capacitance image obtained at a bias voltage of 1.5 V; (b) SCM signal spectra extracted from images obtained at different bias voltages at points labeled A, B, and C in (a); (c) representative single scanning capacitance spectrum; (d) computed capacitance–voltage spectra for InGaN quantum-well structures with In concentrations of 10%, 20%, and 30%; (e) computed capacitance–voltage spectra for $In_{0.15}Ga_{0.85}N$ quantum-well structures with $In_{0.15}Ga_{0.85}N$ thicknesses of 1.5, 2.5, and 3.5 nm.

Spatially resolved scanning capacitance spectroscopy combined with numerical simulations provides insight into the origins of the SCM contrast features observed in Fig. 2. Figure 3(a) shows a 3 $\mu$m × 1 $\mu$m SCM image obtained at a

bias voltage of 1.5 V, in which localized regions of increased SCM signal level are clearly evident. Figure 3(b) shows spatially resolved scanning capacitance spectra for three locations marked within the SCM image, constructed by extracting SCM signal levels from a series of images obtained at different bias voltages. Points A and B correspond to circular regions in which increased SCM signal levels are observed at bias voltages of 1.25–1.75 V, and point C to a region of approximately average signal level at these voltages. A single representative scanning capacitance spectrum measured directly for this sample is shown in Fig. 3(c). A comparison of Figs. 3(b) and 3(c) confirms the validity of SCM signal spectra constructed from image data as in Fig. 3(b).

To interpret the variations in the SCM signal spectra that are evident in Fig. 3(b), we employ numerical simulations of capacitance–voltage spectra, from which the expected SCM signal spectrum is computed.[15] Figure 3(d) shows scanning capacitance spectra computed in this manner for In concentrations in the quantum well of 10%, 20%, and 30%. The differences in voltages at which various spectroscopic features occur experimentally and in such simulations are due primarily to the effects of finite tip size, tip shape, and series resistance in the sample, as analyzed in detail in our prior studies.[15] The similarity of the measured scanning capacitance spectrum in Fig. 3(c) and the simulated spectra in Fig. 3(d), except for the bias voltage ranges, provides validation for this explanation.

A comparison of the experimental SCM signal spectra in Fig. 3(b) with the computed spectra indicates that the increased signal levels observed in circular regions in the SCM images are consistent with a corresponding local increase in In concentration. Specifically, a comparison of the spectra at points A and B with that at point C in Fig. 3 reveals that for points A and B, a higher signal level is observed at relatively low bias voltages, while a lower signal level is measured at higher bias voltages ($\sim$2.0 V and above). As is evident in the simulated SCM signal spectra, this behavior is consistent with the presence of increased local In concentration at points A and B relative to that at point C. Physically, higher local In concentration is expected to lead to the onset of electron accumulation, and consequently an increase in SCM signal level, at lower positive bias voltages due to the higher positive polarization charge at the upper $GaN/In_xGa_{1-x}N$ interface. Figure 3(e) shows simulated SCM signal spectra for quantum wells with varying $In_{0.15}Ga_{0.85}N$ layer thickness, the other major potential source of the inhomogeneities in electronic structure imaged by SCM. As is evident from the figure, variations in quantum-well thickness result in only very minor variations in SCM signal spectra, and may therefore be eliminated as the primary source of the SCM image contrast observed in Figs. 2 and 3(a). Other possible sources, such as variation in local conductivity or surface potential, can be shown by straightforward analysis or routine surface potential measurements (not shown here) to be insufficient to give rise to the observed SCM image contrast.

Our interpretation of the observed SCM contrast as a consequence of local variations in In concentration, and in particular of In clustering in the quantum well, is consistent with (but not dependent on) other studies in which backscattered electron imaging in a scanning electron microscope and analysis of the temperature dependence of the peak quantum-well luminescence energy were used to deduce the presence of In-rich clusters in very similarly grown samples.[10,16] The reported densities of these clusters varied from 2 to 30 $\times 10^9$ cm$^{-2}$ depending on the growth conditions, and our measured densities are well within this range. Furthermore, the apparent presence of In clusters in the quantum-well region was correlated with the observation of dramatically increased photoluminescence efficiency compared to that measured for nominally identical samples grown under conditions for which formation of In-rich regions was not observed, presumably due to enhanced recombination of excitons localized at potential minima created by localized In-rich regions.[16] The studies described here confirm the correlation between increased luminescence efficiency and the presence of In-rich clusters via direct imaging of electron accumulation in these clusters using SCM, and demonstrates an approach for imaging of nanoscale compositional variations in subsurface quantum-well structures.

In summary, we have used scanning capacitance microscopy and spectroscopy combined with detailed numerical simulations to characterize local electronic structure in an $In_{0.15}Ga_{0.85}N/GaN$ quantum-well structure grown by MOCVD. Our studies reveal the presence of nanoscale In-rich regions within the $In_xGa_{1-x}N$ quantum well, typically 25 nm or smaller in radius, with a density of $\sim 8 \times 10^9$ cm$^{-2}$. Within these In-rich regions, electron accumulation at positive tip bias voltages is enhanced, leading to clear, bias-dependent SCM signal contrast. Detailed numerical simulations confirm that the SCM features observed indeed arise primarily from locally increased In concentration rather than other possible nanoscale structural inhomogeneities such as quantum-well thickness variations.

Part of this work was supported by the National Science Foundation (Grant Nos. DMR-0072912 and DMR-0405851).

[1] S. Nakamura and G. Fasol, *The Blue Laser Diode* (Springer, Berlin, 1997).
[2] S. Nakamura, M. Senoh, S.-I. Nagahama, N. Iwasa, T. Yamada, T. Matsushita, H. Kiyoku, Y. Sugimoto, T. Kozaki, H. Umemoto, M. Sano, and K. Chocho, Appl. Phys. Lett. **72**, 211 (1998).
[3] J. L. Sanchez-Rojas, J. A. Garrido, and E. Munoz, Phys. Rev. B **61**, 2773 (2000).
[4] F. A. Ponce, D. Cherns, W. Goetz, and R. S. Kern, Mater. Res. Soc. Symp. Proc. **482**, 453 (1998).
[5] N. Duxbury, U. Bangert, P. Dawson, E. J. Thrush, W. Van der Stricht, K. Jacobs, and I. Moerman, Appl. Phys. Lett. **76**, 1600 (2000).
[6] M. Benamara, Z. Liliental-Weber, W. Swider, J. Washburn, R. D. Dupuis, P. A. Grudowski, C. J. Eiting, J. W. Yang, and M. A. Khan, Mater. Res. Soc. Symp. Proc. **572**, 357 (1999).
[7] S. Chichibu, T. Azuhata, T. Sota, and S. Nakamura, Appl. Phys. Lett. **69**, 4188 (1996).
[8] K. V. Smith, E. T. Yu, J. M. Redwing, and K. S. Boutros, Appl. Phys. Lett. **75**, 2250 (1999).
[9] D. M. Schaadt, E. J. Miller, E. T. Yu, and J. M. Redwing, Appl. Phys. Lett. **78**, 88 (2001).
[10] D. Lu, D. I. Florescu, V. N. Merai, S. Li, J. J. Gardner, M. J. Begarney, and E. A. Armour, Phys. Status Solidi A **202**, 795 (2005).
[11] X. Zhou, E. T. Yu, D. Florescu, J. C. Ramer, D. S. Lee, and E. A. Armour, Appl. Phys. Lett. **85**, 407 (2004).
[12] G. L. Snider, Computer Program 1D Poisson/Schrödinger: A band diagram calculator, University of Notre Dame, Notre Dame, IN, 1995.
[13] H. Zhang, E. J. Miller, E. T. Yu, C. Poblenz, and J. S. Speck, Appl. Phys. Lett. **84**, 4644 (2004).
[14] B. Heying, E. J. Tarsa, C. R. Elsass, P. Fini, S. P. DenBaars, and J. S. Speck, J. Appl. Phys. **85**, 6470 (1999).
[15] D. M. Schaadt and E. T. Yu, J. Vac. Sci. Technol. B **20**, 1671 (2002).
[16] D. I. Florescu, J. C. Ramer, V. N. Merai, A. Parekh, D. Lu, D. S. Lee, and E. A. Armour, J. Cryst. Growth **272**, 449 (2004).